Measurement of Electronic States of PbS Nanocrystal Quantum Dots Using Scanning Tunneling Spectroscopy: The Role of Parity Selection Rules in Optical Absorption

Bogdan Diaconescu,[1] Lazaro A. Padilha,[1] Prashant Nagpal,[1] Brian S. Swartzentruber,[2] and Victor I. Klimov[1,*]

[1]*Center for Advanced Solar Photophysics and Chemistry Division, Los Alamos National Laboratory, Los Alamos, New Mexico 87545, USA*

[2]*Center for Integrated Nanotechnologies, Sandia National Laboratories, Albuquerque, New Mexico 87185, USA*

(Received 9 February 2012; revised manuscript received 11 April 2012; published 22 March 2013)

We study the structure of electronic states in individual PbS nanocrystal quantum dots by scanning tunneling spectroscopy (STS) using one-to-two monolayer nanocrystal films treated with 1, 2-ethanedithiols (EDT). Up to six individual valence and conduction band states are resolved for a range of quantum dot sizes. The measured states' energies are in good agreement with calculations using the $\mathbf{k} \cdot \mathbf{p}$ four-band envelope function formalism. A comparison of STS and optical absorption spectra indicates that some of the absorption features can only be explained by asymmetric transitions involving the states of different symmetries (e.g., S and P or P and D), which points towards the relaxation of the parity selection rules in these nanostructures. STS measurements also reveal a midgap feature, which is likely similar to one observed in previous charge transport studies of EDT-treated quantum dot films.

DOI: 10.1103/PhysRevLett.110.127406 PACS numbers: 78.67.Hc, 68.37.Ef, 78.67.Bf

Nanocrystal (NC) quantum dots are characterized by discrete electronic states with atomlike symmetries and size-controlled energies [1]. Lead chalcogenides such as PbS and PbSe feature a narrow band gap in the mid-infrared and small electron and hole effective masses. As a result, the NCs made of these materials are characterized by strong quantum confinement for both carriers and a wide-range, size-controlled tunability of the band gap energy. This makes these nanostructures attractive materials for applications in solution-processable devices including infrared light emitting diodes, printable field-effect transistors [2,3], and solar cells [4,5].

Electronic structures of lead-salt NCs were initially studied theoretically using a $\mathbf{k} \cdot \mathbf{p}$ four-band envelope function formalism [6], which predicted almost mirror symmetric electronic states in the conduction and valence bands having S, P, D, etc. symmetries. Because of these well-defined symmetries, one-photon interband optical transitions must occur with observation of parity selection rules, according to which only transitions that couple the states of the same symmetry (S_h-S_e, P_h-P_e, etc.; subscripts "e" and "h" stand for electron and hole states, respectively) are allowed. However, this theoretical prediction is at odds with results of optical absorption measurements [7–10] that indicate the presence of intense peaks at energies of asymmetric transitions such as $1S_h - 1P_e$ and $1P_h - 1S_e$. Based on parity selection rules these transitions are forbidden and can be seen only in two-photon but *not* single-photon absorption. This inconsistency has lead to intense and still continuing debates on the interpretation of various absorption features in samples of PbSe and PbS quantum dots [9–13].

One approach to resolve this problem has been to include the anisotropy of electron and hole masses in the model [11,12,14,15]. The effects of anisotropy result in splitting of electronic states, which places one of the split-off $1P_h - 1P_e$ parity conserving transitions near the nominally forbidden $1S_h - 1P_e$ and $1P_h - 1S_e$ transitions. This seems to help reconcile the discrepancy between the theory and the experiment for PbSe NCs [14], however, *not* for PbS quantum dots as in this material the splitting due to anisotropy is too small [12,15] to explain experimental observations. Another suggested way to resolve this problem has been to allow for a breakdown of parity conservation by introducing inversion asymmetry in the wave functions of lead-salt NCs (see, e.g., Ref. [13]).

Previous experimental works have attempted to elucidate the nature of optical transitions in lead-salt quantum dots by applying both optical [9,10,16] and scanning tunneling spectroscopy (STS) measurements [17,18]. These studies, however, mostly focused on PbSe NCs and therefore, could not conclusively answer the question on the "strictness" of parity selection rules, because strong band anisotropies in PbSe complicate the interpretation of optical spectra. PbS NCs have more isotropic bands and almost identical electron and hole effective masses that make them more suitable for separating the effects due to anisotropy from those due to breakdown of parity conservation. The studies that would compare the energies of electronic states in PbS NCs measured by STS and those obtained from optical spectroscopy, however, are still lacking.

Here, we fill this gap by conducting STS measurements on individual PbS NCs of various sizes and compare them to the results of optical measurements. We observe that some of the features in single-photon absorption can only be described by asymmetric transitions that couple, for example, S and P or P and D states. This observation strongly suggests the relaxation of parity conservation in PbS NCs due, e.g., to an internal electric field or an

asymmetric distribution of atoms relative to the NC center as suggested in Ref. [13].

In our studies, we use PbS NCs with oleylamine capping synthesized according to Ref. [19]. The NCs were dispersed in octane and then spin cast onto a glass substrate coated with indium tin oxide (0.5–1 kΩ/cm resistivity). The substrates were cleaned by immersion into a 1:1:1 solution of iso-propanol, methanol, and acetone, sonicated for 5 min, and then dried in a stream of nitrogen gas. The NC film was treated with 1, 2-ethanedithiols (EDT), the procedure which links NCs into a weakly conducting network as described in Ref. [20]. The final film thickness was one to two NC monolayers. The samples were introduced into the vacuum chamber and then annealed for about 4 h at 110 °C in ultrahigh vacuum (UHV) to remove unbounded ligands and solvent molecules.

We studied four different samples from two batches with the photoluminescence (PL) bands at 1100 and 1400 nm. Scanning tunneling microscopy (STM) and transmission electron microscopy studies [Figs. 1(a) and 1(b), respectively] indicated a relatively broad NC size distribution, which allowed us to perform the measurements across a fairly large range of sizes corresponding to the band gap energies (E_g) from 0.7 to 1.2 eV. The STS studies were conducted at 100 K in a UHV chamber with base pressure $<1 \times 10^{-10}$ torr using a modified commercial variable-temperature STM system (RHK-300). The tunneling current noise levels were smaller than 1 pA peak-to-peak over the full bandwidth. Etched polycrystalline tungsten tips were used. The oxide layer on the tip was removed via Ne^+ sputtering after the introduction into the UHV chamber and then the tips were sharpened and annealed in the field emission regime to improve their stability.

In our studies, the samples were cooled down to 100 K; however, the STM tip remained close to room temperature, which limited energy resolution to ~20–30 meV. In the STS measurements, the tip was placed above the center of the individual NC, the feedback loop was disconnected, and the tunneling current I was recorded as a function of tip-substrate bias V. We typically acquired 30–70 spectra for the same NC to verify for reproducibility and then averaged them to increase the signal-to-noise ratio.

We used two STS techniques: a constant gap method [21,22], in which the tunneling junction width was maintained constant during the bias voltage sweep [Fig. 1(c)], and a variable gap sweep method [23] where the junction width decreased proportionally with the bias voltage [Fig. 1(d)]. For both techniques the recorded spectra exhibited well-resolved, tunneling resonances on both sides of the band gap. However, the variable-gap method was more suitable for mapping the high-energy states than the constant-gap method, because in the latter case the tunneling junction would often become unstable at high currents. Also, the variable-gap measurements allowed for a better signal-to-noise ratio in the band-edge regions. Based of these observations, all measurements shown below were conducted using the variable-gap technique.

Changes in the NC-tip distance utilized in this technique can, in principle, affect the positions of the measured peaks due to changes in the NC-tip capacitance ($C_{\text{Tip-NC}}$), which together with the NC-substrate capacitance ($C_{\text{NC-Sub}}$) define the fraction (η) of the tip-substrate bias (V) that

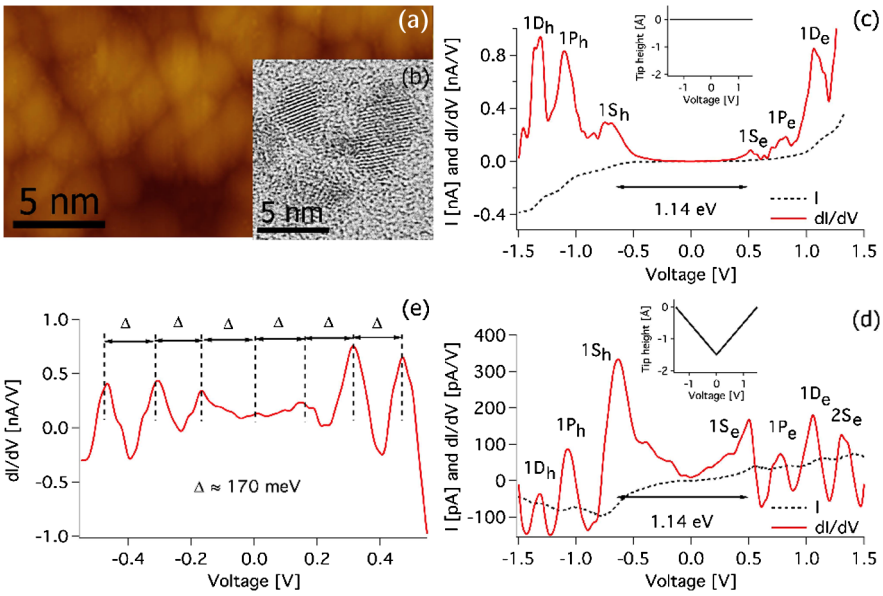

FIG. 1 (color online). STM/STS measurements of PbS NCs. (a) An STM constant current image of PbS NCs on the ITO/glass substrate. (b) A transmission electron microscopy image of PbS NCs. (c) Single-dot constant height (inset) I/V (dashed line) and dI/dV (solid line) spectra showing the first three electron and hole states. (d) Variable-gap (inset) I/V (dashed line) and dI/dV (solid line) spectra for the same dot. (e) STS showing charging effects in the case of high tunneling current (> 700 pA). STM/STS data were acquired at sample temperature of 100 K.

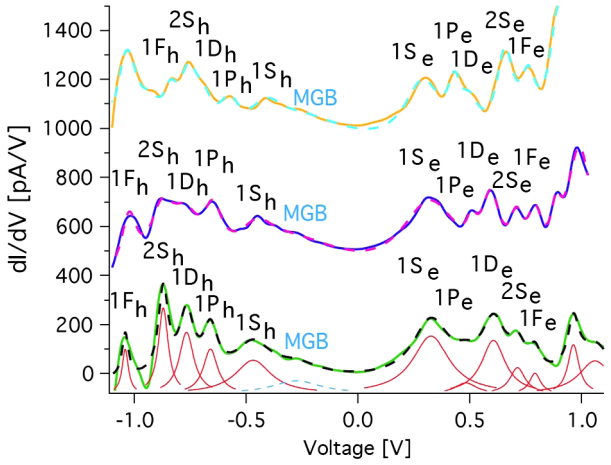

FIG. 2 (color online). dI/dV spectra for three different PbS NCs with band gap energies of 0.65 eV (upper trace; apparent STS band gap $\Delta V_{NC} = 0.70$ eV), 0.69 eV (intermediate trace, $\Delta V_{NC} = 0.74$ eV), and 0.75 eV (lower trace, $\Delta V_{NC} = 0.81$ eV). In these spectra, we resolve at least six electron and five hole states. The measured spectra (solid lines) are fit (dashed lines) using a sum of Lorentzians used to identify individual hole and electron states (shown at the bottom by solid red lines). The asymmetric background in the band-gap region can be attributed to the manifold of mid-gap states (MGB) shown by the blue dashed line.

is applied to the NC: $V_{NC} = \eta V$, where $\eta = C_{NC\text{-}Sub}/(C_{NC\text{-}Sub} + C_{Tip\text{-}NC})$ [24,25]. In our weakly conductive samples, however, the correction for bias division is insignificant as each NC probed by the STM has direct electrical contact to the substrate, which corresponds to $C_{NC\text{-}Sub} \rightarrow \infty$ and $\eta \rightarrow 1$. This assessment is confirmed by the comparison of the STS spectra collected using either a constant or a variable-gap method [Figs. 1(c) and 1(d)]. The positions of the STS peaks in these spectra are virtually identical suggesting that independent of the tip-NC separation, $C_{NC\text{-}Sub}$ is always much greater than $C_{Tip\text{-}NC}$ and hence $\eta \approx 1$ (see Supplemental Material for more details [26]).

In the STS studies, the tunneling junction gap width typically varied between 1 and 2 Å/V. The spectra were essentially unchanged when the tunneling set-point conditions were within 1.0–1.5 V for the bias and 20–300 pA for the current. However, increasing the set-point current to more than 700 pA resulted in the appearance of multiple, equally spaced tunneling resonances [Fig. 1(e)] that developed due to discrete electron charging of the NC similar to that reported in Ref. [27]. All STS data presented below were acquired below this threshold and reflected, therefore, the single-particle density of states recorded in the regime of shell tunneling.

The STS spectra were analyzed by fitting them to a sum of multiple Lorentzians, which allowed us to accurately identify the positions of individual states even in the case of overlapping spectral features (see Supplemental Material [26]). This procedure is illustrated in Fig. 2, where we display the dI/dV spectra for three NCs with different energy gaps.

One interesting observation is that the background between the band-edge $1S_e$ and $1S_h$ peaks is asymmetric indicating the presence of a broad midgap band (MGB) at around 0.2–0.3 eV above the $1S_h$ state (blue dashed line at the bottom of Fig. 2). Interestingly, while the peaks outside the band gap exhibit a pronounced dependence on NC dimensions and hence E_g [see Fig. 3(a)], the intragap feature has the same energy (~ 0.27 eV below the Fermi level) for all NC sizes [see Fig. 3(a); stars]. This size independence suggests that the states responsible for intragap tunneling are likely associated with the network of surface defects that are similar to those detected in a recent charge transport study of PbS NC films prepared using the same EDT treatment procedure as one in the present experiments [20].

In our analysis of the STS data, we account for the electron polarization energy, Σ, [24,25], which is responsible for the increase of the apparent (measured) energy of the STS peak compared to the true energy of a given electronic state. Our calculations indicate that Σ increases with decreasing NC size (see Supplemental Material [26]); however, even for the smallest NCs studied here, it does not exceed 50 meV. All electronic energies shown below were derived from raw STS data by introducing a correction for Σ [24,25].

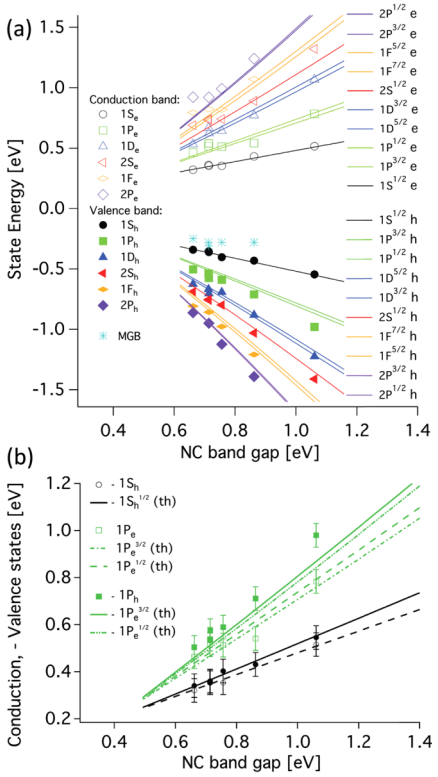

FIG. 3 (color online). (a) Individual states' energies derived from the STS data corrected for the contribution from the polarization energy (symbols) as a function of true NC band-gap energy. Lines are theoretical calculations using the $\mathbf{k} \cdot \mathbf{p}$ four-band envelope function formalism. (b) The comparison of the energies of the first two conduction- and valence-band states plotted as a function of NC band-gap energy. Experimental data are shown by symbols while theoretical calculations by lines.

We start our analysis of the STS measurements with the two lowest-energy conduction and valence band peaks. In Fig. 3(b), we plot the positions of these peaks as a function of the $1S_e - 1S_h$ spacing, which provides a direct measure of E_g. We further compare them to the calculations [lines in Fig. 3(a)] conducted using the isotropic $\mathbf{k} \cdot \mathbf{p}$ four-band envelope function formalism [6], in which a NC is approximated by a sphere with an infinite potential barrier [25]. This model overestimates the states' energies for a given quantum dot size [6]. However, it still allows for a fairly accurate comparison with the experiment if both the measurements and the calculations are plotted not as a function of NC size but E_g, an approach used, for example, in Ref. [28].

Because of the similarity between the electron and hole effective masses in PbS [6], and highly isotropic bands [15], one can expect that the energies of same-type conduction and valence band states should also be similar (i.e., "mirror symmetric"). Indeed, the measurements in Fig. 3(b) (symbols) indicate that the first and the second electron states are close to corresponding hole states. Further, the comparison with the theory [lines in Fig. 3(a)] indicates that the energies of the first and the second STS peaks are close to the calculations for the $1S^{1/2}$ and $1P^{1/2}/1P^{3/2}$ levels, respectively. While here and below, in our modeling we account for the effect of the total angular momentum (shown by the superscript) on the state's energy, the corresponding energy splittings are too small (< 20 meV) to be resolved experimentally.

In addition to the two lowest-energy quantum-confined states, the STS allows us to measure 3–4 higher energy levels for both electrons and holes. We plot the positions of all STS peaks in Fig. 3(a) (symbols) and compare them to the results of the $\mathbf{k} \cdot \mathbf{p}$ calculations (lines). As in the case of the lower energy features, we observe a remarkable agreement between the calculations and the measurements for higher energy peaks, which allows us to assign the third and the fourth STS features to the $1D$ and $2S$ states, respectively. For the larger NCs (smaller energy gap), we can even resolve the fifth and the six peaks that likely correspond to the $1F$ and $2P$ levels, respectively.

Next, we use the energies of electronic states derived from the STS measurements to address the problem of classification of optical transitions in PbS NCs. For this purpose, we compare the energies of the second, third and fourth single-photon optical transitions from Ref. [10] (the notation of these transitions is illustrated in Fig. 4(a) using the PL excitation spectrum of the ensemble sample

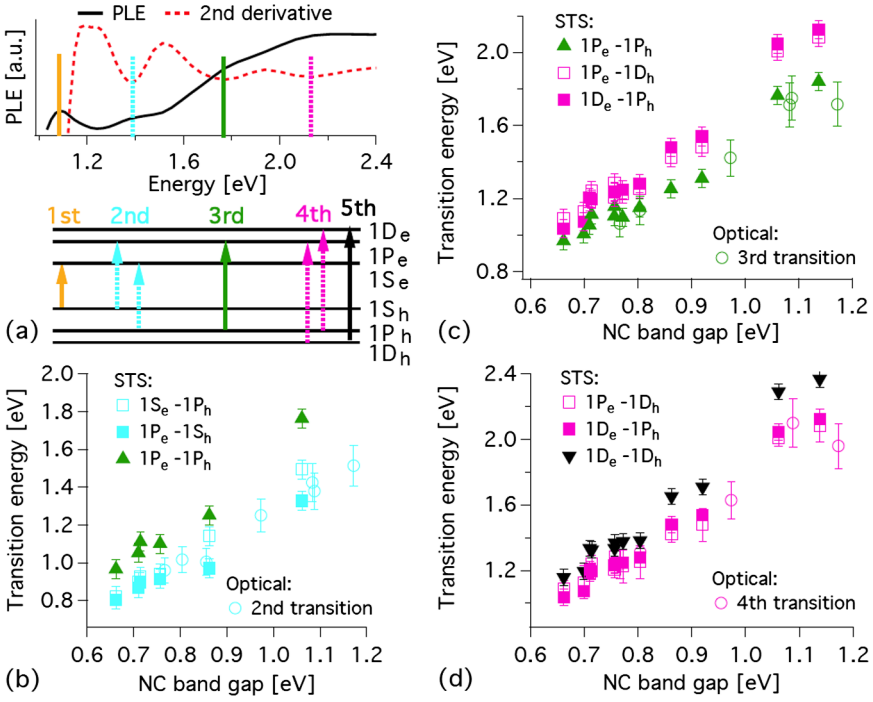

FIG. 4 (color online). (a) The first four optical transitions observed in the PL excitation (PLE) spectrum (solid line) and its second derivative (dashed line) of the sample with $E_g = 1.09$ eV. (b–d) The comparison of energies of various symmetric and asymmetric interband transitions derived from the STS measurements (squares and triangles) and optical transitions (circles) from the PLE and single-photon absorption spectra (optical data are from Ref. [10]). Based on this comparison, the 2nd peak in the optical spectra (open circles in 'b') is best described by the asymmetric STS $1S_e - 1P_h$ and $1P_e - 1S_h$ transitions (open and solid squares in 'b', respectively). On the other hand, the 3rd optical transition (open circles in 'c') corresponds to the symmetric $1P_e - 1P_h$ STS transition (solid triangles). Finally, the 4th optical transition (open circles in 'd') is close to the asymmetric STS $1P_e - 1D_h$ and $1D_e - 1P_h$ STS transitions (open and solid squares in 'd', respectively).

with $E_g = 1.09$ eV) with the energies of the symmetric (parity conserving) and asymmetric (not parity conserving) transitions derived by STS [see Figs. 4(b)–4(d)]. The results of this comparison indicate that the second optical feature is closer to the asymmetric $1S_e - 1P_h$ and $1P_e - 1S_h$ transitions [Fig. 4(b)] than to the symmetric one ($1P_e - 1P_h$), suggesting that parity conservation is *not* strictly observed in PbS NCs. On the other hand, the position of the third optical feature agrees well with the position of the symmetric $1P_e - 1P_h$ transition [Fig. 4(c)]. However, the closeness of the fourth optical feature to the positions of the asymmetric $1D_e - 1P_h$ and $1P_e - 1D_h$ transitions again suggests the breakdown of parity conservation [Fig. 4(d)]. These results demonstrate that the parity selection rules are relaxed in PbS NCs and further suggest that the band anisotropy does not have to be necessarily invoked to explain the appearance of asymmetric transitions. A possible reason for the breakdown of parity conservation is the existence of internal electric field in these NCs. While no direct measurements of internal electric fields in PbS quantum dots are available in the literature, previous studies of II-VI NCs with both cubic and hexagonal lattice structures [29,30] indicate that they can exhibit a large dipole moment and hence strong internal electric field, which was attributed to surface-localized electrical charges [29]. As was suggested in Ref. [13], an additional reason for the breakdown of wave function inversion symmetry in lead-salt quantum dots could be the displacement of the center of a NC with respect to an atomic site.

To summarize, we have conducted STS studies of individual PbS NCs with E_g between 0.7 and 1.2 eV. Using this method, we resolve up to six quantum-confined states in both conduction and valence bands and states' energies agree well with the $\mathbf{k} \cdot \mathbf{p}$ calculations. The comparison between the STS and optical measurements indicates that parity selection rules are relaxed in PbS NCs, which leads to the appearance of strong optical absorption features due to transitions that do not conserve parity. Specifically, we show that the second and the forth optical absorption features can be explained by asymmetric $1S - 1P$ and $1P - 1D$ transitions that would be forbidden in the case of strict observation of parity conservation. In addition to intrinsic NC states, STS measurements reveal a broad midgap band whose position (~ 0.27 eV below the Fermi level) is not significantly affected by the NC size. The states responsible for this feature are likely associated with the network of surface defects that are similar to those observed in recent charge transport measurements of EDT-treated PbS NC films [20].

This work was supported by the Center for Advanced Solar Photophysics, an Energy Frontier Research Center funded by the U.S. Department of Energy (DOE), Office of Science (OS), Office of Basic Energy Sciences (OBES). The STM measurements were conducted at the Sandia site of the Center for Integrated Nanotechnologies, a user facility of U.S. DOE, OBES.

*klimov@lanl.gov

[1] A. P. Alivisatos, Science **271**, 933 (1996).
[2] T. S. Mentzel, V. J. Porter, S. Geyer, K. MacLean, M. G. Bawendi, and M. A. Kastner, Phys. Rev. B **77**, 075316 (2008).
[3] D. V. Talapin and C. B. Murray, Science **310**, 86 (2005).
[4] J. M. Luther, J. B. Gao, M. T. Lloyd, O. E. Semonin, M. C. Beard, and A. J. Nozik, Adv. Mater. **22**, 3704 (2010).
[5] J. Tang, K. W. Kemp, S. Hoogland, K. S. Jeong, H. Liu, L. Levina, M. Furukawa, X. H. Wang, R. Debnath, D. K. Cha, K. W. Chou, A. Fischer, A. Amassian, J. B. Asbury, and E. H. Sargent, Nat. Mater. **10**, 765 (2011).
[6] I. Kang and F. W. Wise, J. Opt. Soc. Am. B **14**, 1632 (1997).
[7] H. Du, C. Chen, R. Krishnan, T. D. Krauss, J. M. Harbold, F. W. Wise, M. G. Thomas, and J. Silcox, Nano Lett. **2**, 1321 (2002).
[8] B. L. Wehrenberg, C. J. Wang, and P. Guyot-Sionnest, J. Phys. Chem. B **106**, 10634 (2002).
[9] J. J. Peterson, L. Huang, C. Delerue, G. Allan, and T. D. Krauss, Nano Lett. **7**, 3827 (2007).
[10] G. Nootz, L. A. Padilha, P. D. Olszak, S. Webster, D. J. Hagan, E. W. Van Stryland, L. Levina, V. Sukhovatkin, L. Brzozowski, and E. H. Sargent, Nano Lett. **10**, 3577 (2010).
[11] J. M. An, A. Franceschetti, S. V. Dudiy, and A. Zunger, Nano Lett. **6**, 2728 (2006).
[12] A. Franceschetti, J. W. Luo, J. M. An, and A. Zunger, Phys. Rev. B **79**, 241311 (2009).
[13] S. V. Goupalov, Phys. Rev. B **79**, 233305 (2009).
[14] A. D. Andreev and A. A. Lipovskii, Phys. Rev. B **59**, 15402 (1999).
[15] G. E. Tudury, M. V. Marquezini, L. G. Ferreira, L. C. Barbosa, and C. L. Cesar, Phys. Rev. B **62**, 7357 (2000).
[16] M. T. Trinh, A. J. Houtepen, J. M. Schins, J. Piris, and L. D. A. Siebbeles, Nano Lett. **8**, 2112 (2008).
[17] P. Liljeroth, P. A. Z. van Emmichoven, S. G. Hickey, H. Weller, B. Grandidier, G. Allan, and D. Vanmaekelbergh, Phys. Rev. Lett. **95**, 086801 (2005).
[18] G. A. Grinbom, M. Saraf, C. Saguy, A. C. Bartnik, F. Wise, and E. Lifshitz, Phys. Rev. B **81**, 245301 (2010).
[19] M. A. Hines and G. D. Scholes, Adv. Mater. **15**, 1844 (2003).
[20] P. Nagpal and V. I. Klimov, Nat. Commun. **2**, 486 (2011).
[21] U. Banin, Y. W. Cao, D. Katz, and O. Millo, Nature (London) **400**, 542 (1999).
[22] E. P. A. M. Bakkers, Z. Hens, A. Zunger, A. Franceschetti, L. P. Kouwenhoven, L. Gurevich, and D. Vanmaekelbergh, Nano Lett. **1**, 551 (2001).
[23] P. Mårtensson and R. M. Feenstra, Phys. Rev. B **39**, 7744 (1989).
[24] Y. M. Niquet, C. Delerue, G. Allan, and M. Lannoo, Phys. Rev. B **65**, 165334 (2002).
[25] G. A. Grinbom, M. Saraf, C. Saguy, A. C. Bartnik, F. Wise, and E. Lifshitz, Phys. Rev. B **81**, 245301 (2010).
[26] See Supplemental Material at http://link.aps.org/supplemental/10.1103/PhysRevLett.110.127406 for the details of the analysis of STS spectra.
[27] P. Jiang, Z. F. Liu, and S. M. Cai, J. Appl. Phys. **90**, 2039 (2001).
[28] D. J. Norris and M. G. Bawendi, Phys. Rev. B **53**, 16338 (1996).
[29] M. Shim and P. Guyot-Sionnest, J. Chem. Phys. **111**, 6955 (1999).
[30] S. A. Blanton, R. L. Leheny, M. A. Hines, and P. Guyot-Sionnest, Phys. Rev. Lett. **79**, 865 (1997).